

Diffusion enhancement in bacterial cytoplasm through an active random force

Lingyu Meng¹, Yiteng Jin², Yichao Guan³, Jiayi Xu⁴, and Jie Lin^{1,2,*}

¹*Peking-Tsinghua Center for Life Sciences, Academy for Advanced Interdisciplinary Studies, Peking University, Beijing 100871, China*

²*Center for Quantitative Biology, Academy for Advanced Interdisciplinary Studies, Peking University, Beijing 100871, China*

³*The Graduate Program in Biophysical Sciences, University of Chicago, Chicago, Illinois 60637, USA*

⁴*Yuanpei College, Peking University, Beijing 100871, China*



(Received 5 September 2022; accepted 10 July 2023; published 7 August 2023)

Experiments have found that diffusion in metabolically active cells is much faster than in dormant cells, especially for large particles. However, the mechanism of this size-dependent diffusion enhancement in living cells is still unclear. In this Letter, we approximate the net effect of metabolic processes as a white-noise active force and simulate a model system of bacterial cytoplasm with a highly polydisperse particle size distribution. We find that diffusion enhancement in active cells relative to dormant cells can be more substantial for large particles. Our simulations agree quantitatively with the experimental data of *Escherichia coli*, suggesting an autocorrelation function of the active force proportional to the cube of the particle radius. We demonstrate that such a white-noise active force is equivalent to an active force of about 0.57 pN with random orientation. Our work unveils an emergent simplicity of random processes inside living cells.

DOI: [10.1103/PhysRevResearch.5.L032018](https://doi.org/10.1103/PhysRevResearch.5.L032018)

The efficient diffusion of cellular components is crucial for various biological processes in bacteria since they do not have active transport systems involving protein motors and cytoskeletal filaments [1–4]. Meanwhile, bacterial cytoplasm is highly crowded [5–8]. Particle diffusion inside the bacterial cytoplasm is significantly suppressed compared with a dilute solution [9–14]. Interestingly, the diffusion of large cellular components, such as plasmids, protein filaments, and storage granules, turns out to be much faster in metabolically active cells than in dormant cells, i.e., cells depleted of ATP [15–19]. Cellular metabolic activities appear to fluidize the cytoplasm and allow large components to sample cytoplasmic space. Another important feature of bacterial cytoplasm is its polydispersity with constituent sizes spanning from subnanometer to micrometers [20–23]. Intriguingly, diffusion enhancement of a metabolically active cell relative to a dormant cell is size dependent as large components' diffusion constants are much more significantly increased while small molecules diffuse with virtually the same diffusion constants in active and dormant cells [16].

The physical mechanism underlying the size-dependent diffusion behaviors in active cells is far from clear. Because of the numerous ATP-consuming processes *in vivo*, finding the dominant biological processes that speed up diffusion may be difficult or even impossible. In a passive solution, particles receive random kicks from neighboring molecules

due to thermal fluctuation. Therefore, the thermal noise's amplitude is proportional to the temperature according to the fluctuation-dissipation (FD) theorem. In contrast, in the cytoplasm of a metabolically active cell, particles also receive random kicks from biomolecules such as ATPs, amino acids, and other metabolites that do not follow a detailed balance and are therefore out of equilibrium [24–27]. As a result, the net effect of their random collision with a particle is a random force not constrained by the FD theorem.

In this Letter, we simulate a model system of bacterial cytoplasm and adopt a coarse-grained approach by introducing an active random force as the net effect of multiple active processes in cells. We model this active random force as white noise with an amplitude independent of temperature. Our system is highly polydisperse, and according to the Stokes-Einstein relation, the autocorrelation function of the thermal random force is proportional to the particle radius. Inspired by that, we set the autocorrelation function of the active random force proportional to a power-law function of the particle radius. We find that in both passive systems without an active force (corresponding to dormant cells) and active systems (corresponding to metabolically active cells), the diffusion constants are reduced under high density compared with the dilute limit. This diffusion reduction is stronger for larger particles in both passive and active systems.

Nevertheless, the enhancements of diffusion constants in active cells relative to dormant cells can be more substantial for larger particles given an appropriate size-dependent active random force. Most importantly, the experimentally measured ratios of diffusion constants between active and dormant *E. coli* cells agree quantitatively with our simulations and suggest an autocorrelation function of the active random force proportional to the cube of the particle radius. We further demonstrate that such a white-noise active force is equivalent

*Corresponding author: linjie@pku.edu.cn

Published by the American Physical Society under the terms of the [Creative Commons Attribution 4.0 International](https://creativecommons.org/licenses/by/4.0/) license. Further distribution of this work must maintain attribution to the author(s) and the published article's title, journal citation, and DOI.

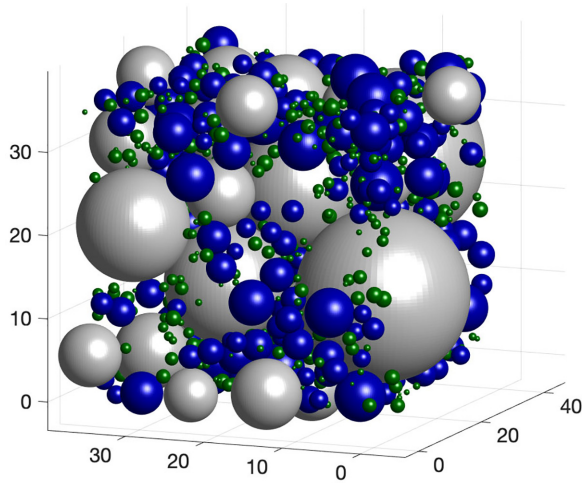


FIG. 1. A snapshot of three-dimensional simulations using polydisperse spheres as a model system of the bacterial cytoplasm. In this example, the volume fraction $\phi = 0.58$. Particles are colored according to their sizes.

lent to an active force with a constant magnitude undergoing rotational diffusion. From the data of *E. coli*, we infer the magnitude of this active force as 0.57 pN, consistent with typical force magnitudes in the cytoplasm [28]. Our results shed light on the mechanical nature of out-of-equilibrium processes in the bacterial cytoplasm and unveil an emergent simplicity in complex living systems.

Size-dependent active random force. We model the various cellular components by spherical particles with heterogeneous radii to mimic the polydisperse cytoplasm (Fig. 1) and their equations of motion using the Langevin dynamics,

$$\eta_i \frac{dr_{i,\alpha}}{dt} = -\frac{\partial U}{\partial r_{i,\alpha}} + \xi_{i,\alpha} + \kappa_{i,\alpha}. \quad (1)$$

Here, $i = 1, 2, \dots, N$ where N is the number of particles and $\alpha = x, y, z$ the directions in the Cartesian coordinate. η_i is the friction coefficient of the i th particle and obeys the Stokes' law $\eta_i = 6\pi\nu a_i$, where a_i is the radius, and ν is the viscosity of the background solvent. U is the pairwise interaction between particles which we model as $U = \frac{1}{2} \sum_{i \neq j} k(a_i + a_j - r_{ij})^2 \Theta(a_i + a_j - r_{ij})$ where $r_{ij} = |\mathbf{r}_i - \mathbf{r}_j|$ and Θ is the Heaviside step function: Particles repel each other only when they overlap. $\xi_{i,\alpha}$ is the thermal noise, and its autocorrelation function obeys the FD theorem [29]

$$\langle \xi_{i,\alpha}(t) \xi_{j,\beta}(t') \rangle = 12\pi\nu a_i k_B T \delta_{ij} \delta_{\alpha\beta} \delta(t - t'). \quad (2)$$

Here, k_B is the Boltzmann constant, and T is the temperature. We introduce an active random force $\kappa_{i,\alpha}$ as the coarse-grained outcome of active processes in a metabolically active cell, and its autocorrelation function is independent of temperature,

$$\langle \kappa_{i,\alpha}(t) \kappa_{j,\beta}(t') \rangle = 2A\tilde{a}_i^\gamma \delta_{ij} \delta_{\alpha\beta} \delta(t - t'). \quad (3)$$

Here, we assume that the noise amplitude is a power-law function of the particle radius where A and γ are constants. Later, we will show that this size dependence of active random force is consistent with experimental measurements.

To nondimensionalize the model, we choose the average particle radius a_0 , the thermal energy $k_B T$, and $t_0 =$

$6\pi\nu a_0^3/k_B T$ as the length, energy, and time unit, respectively. The dimensionless equation of motion becomes

$$\frac{d\tilde{r}_{i,\alpha}}{d\tilde{t}} = -\frac{1}{\tilde{a}_i} \frac{\partial \tilde{U}}{\partial \tilde{r}_{i,\alpha}} + \tilde{\xi}_{i,\alpha} + \tilde{\kappa}_{i,\alpha}, \quad (4)$$

where $\tilde{\xi}_{i,\alpha}$ is the dimensionless thermal noise with its autocorrelation function $\langle \tilde{\xi}_{i,\alpha}(\tilde{t}), \tilde{\xi}_{j,\beta}(\tilde{t}') \rangle = 2\tilde{a}_i^{-1} \delta_{ij} \delta_{\alpha\beta} \delta(\tilde{t} - \tilde{t}')$, and $\tilde{\kappa}_{i,\alpha}$ is the dimensionless active noise with its autocorrelation function $\langle \tilde{\kappa}_{i,\alpha}(\tilde{t}), \tilde{\kappa}_{j,\beta}(\tilde{t}') \rangle = 2\tilde{A}\tilde{a}_i^{\gamma-2} \delta_{ij} \delta_{\alpha\beta} \delta(\tilde{t} - \tilde{t}')$. Here, the dimensionless active noise amplitude $\tilde{A} = Aa_0^{\gamma-1}/(6\pi\nu k_B T)$. In the following, variables with a tilde above are dimensionless. We simulate N particles in a three-dimensional cubic box with a dimensionless side length \tilde{L} under the periodic boundary condition. The N particles' radii obey a shifted lognormal distribution $\tilde{a} = \tilde{a}_{\min} + \exp[\mu + \sigma\mathcal{N}(0, 1)]$, where $\mathcal{N}(0, 1)$ is a standard normal random number, and μ and σ are constants. The minimum radius \tilde{a}_{\min} is 0.1. We set $\sigma = 0.85$ to mimic the polydisperse environment and choose μ by setting the dimensionless average radius $\tilde{a}_{\text{mean}} = \tilde{a}_{\min} + \exp(\mu + \sigma^2/2)$ as 1. We set the physical value of the average radius as $a_0 = 10$ nm, so the particles' radii cover two orders of magnitude, from 1 to about 100 nm, consistent with real bacterial cytoplasm [9,16]. We fix the volume fraction ϕ in each simulation. We also set $T = 300$ K and choose a large dimensionless spring constant $\tilde{k} = 1000$ to mimic a hard-sphere system. The total simulation time \tilde{t}_{tot} is 10 000 with a time step $d\tilde{t} = 2 \times 10^{-4}$.

Active noise facilitates diffusion of large particles. We first investigate the effects of volume fractions on the diffusion constants relative to the dilute limit for both passive and active systems. We compute the diffusion constant for each particle from the time-averaged mean square displacement (MSD) as $D = \langle \Delta \tilde{\mathbf{r}}^2(\Delta \tilde{t}) \rangle / 6\Delta \tilde{t}$ with $\Delta \tilde{t} = 1$ where $\Delta \tilde{\mathbf{r}}(\Delta \tilde{t})$ is the displacement vector during a time interval $\Delta \tilde{t}$. We choose multiple values of ϕ , including 0.58 and 0.64, the critical volume fractions of the glass transition, and random close packing of a monodisperse system in three dimensions [30].

In the dilute limit, collisions between particles are negligible, and the diffusion constant of an active particle with a dimensionless radius \tilde{a} becomes $D_{\text{dilute}} = 1/\tilde{a} + \tilde{A}\tilde{a}^{\gamma-2}$. For a passive particle with $\tilde{A} = 0$, $D_{0,\text{dilute}} = 1/\tilde{a}$. In both passive and active systems, the reduction of diffusion constants in high-volume fractions relative to the dilute limit is more significant for larger particles [Figs. 2(a) and 2(b)]. To demonstrate the effects of active random force, we compare the diffusion constants of active and passive systems in the same volume fraction, which is more biologically relevant. In the dilute limit, the ratio of diffusion constants between active and dormant cells is

$$\frac{D_{\text{dilute}}}{D_{0,\text{dilute}}} = 1 + \tilde{A}\tilde{a}^{\gamma-1}. \quad (5)$$

Our simulation results for $\phi = 0.01$ confirm Eq. (5) [Fig. 2(c)].

For systems with high volume fractions, neither D with $\tilde{A} > 0$ nor D_0 with $\tilde{A} = 0$ is equal to the dilute limit prediction [Figs. 2(a) and 2(b)]. Intriguingly, we find that the simulation results of $D/D_0 - 1$ with high volume fractions still agree reasonably well with the theoretical prediction from the dilute limit, particularly for small particles with $\tilde{a} < 1$ [Fig. 2(d)].

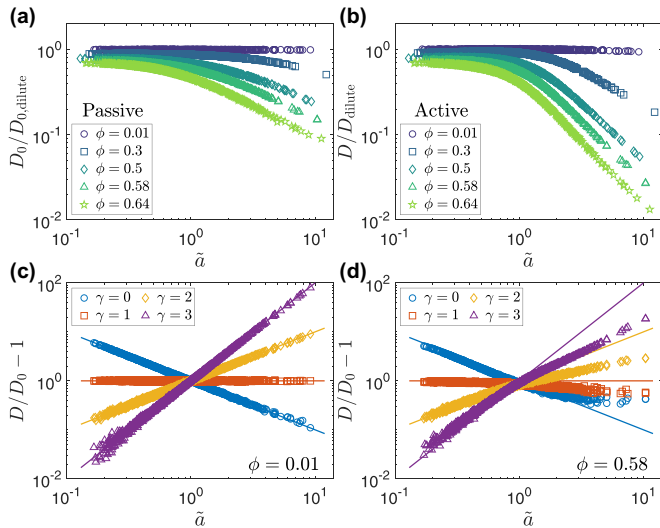


FIG. 2. Diffusion constants of the simulated polydisperse systems. (a) The diffusion constants of passive systems relative to the dilute limit. \tilde{a} is the dimensionless radius. (b) The same analysis as (a) but for an active system. Here, $\tilde{A} = 1$, $\gamma = 3$. The diffusion constants in the dilute limit differ in (a) and (b). (c) $D/D_0 - 1$ for different γ 's. D is the diffusion constant of the active system, and D_0 is the diffusion constant of the passive system. Here, $\phi = 0.01$, $\tilde{A} = 1$. The lines with corresponding colors are the predictions in the dilute limit. (d) The same analysis as (c) but for systems with $\phi = 0.58$. In all panels, $N = 1000$.

The above observation is nontrivial because all particles' diffusion constants deviate from the dilute limit regardless of size [Figs. 2(a) and 2(b)]. Deviations are observed for large particles, and we define an effective γ_{eff} for large particles with $\tilde{a} > 1.2$ such that $D/D_0 - 1 \sim \tilde{a}^{\gamma_{\text{eff}} - 1}$ (see Supplemental Material [31], Fig. S1). Experimentally, the diffusion constants of small particles are close in active and dormant cells; however, the diffusions of large particles are much faster in active cells than in dormant cells [16]. Our simulations in the regime of $\gamma > 1$ agree with experiments [Fig. 2(d)].

We also compute the diffusion constant $D = \langle \Delta \tilde{\mathbf{r}}^2(\Delta \tilde{t}) \rangle / 6\Delta \tilde{t}$ using a longer $\Delta \tilde{t}$ where $\langle \Delta \tilde{\mathbf{r}}^2(\Delta \tilde{t}) \rangle = \tilde{L}^2/32$ but still short enough to ensure that the finite system size does not confine the particles' MSDs, and our conclusions are equally valid under this definition [Figs. S2(a), S2(b), and S3]. We also compute the diffusion constants by fitting the MSDs using $\langle \Delta \tilde{\mathbf{r}}^2(\Delta \tilde{t}) \rangle = 6D\Delta \tilde{t}$ and obtain similar results [Figs. S2(c) and S2(d)].

We track the trajectories of single particles (Fig. 3). We find that particles with small radii can equally explore the system in active and passive systems; however, particles with large radii can only explore space in active systems and remain localized in passive systems, consistent with experimental observations [16].

Comparison with experiments. In Ref. [16], the authors measured the MSDs of exogenous particles of multiple sizes in active and dormant cells, including GFP- μ NS particles, which are GFP-labeled self-assembling avian reovirus proteins with changeable sizes, and mini-RK2 plasmid, which is an engineered low-copy-number plasmid in *E. coli*. We find

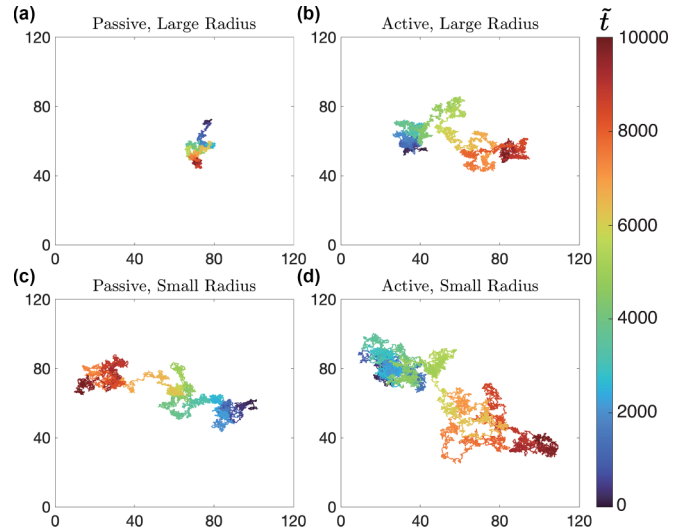


FIG. 3. Single particles' trajectories projected to two dimensions. (a) The trajectory of a large particle with $\tilde{a} = 6.75$ in a passive system. The color represents the time elapsed from the beginning of the trajectory. (b) The trajectory of the same particle in (a) but in an active system. (c) The trajectory of a small particle with $\tilde{a} = 2.44$ in a passive system. (d) The trajectory of the same particle in (c) but in an active system. In (b) and (d), $\tilde{A} = 0.42$ and $\gamma = 3$. In all panels, $\phi = 0.58$, $N = 1000$.

that the measured MSDs are subject to large noises, making it difficult to compute the diffusion constants accurately. To circumvent this problem, we compute the ratios of MSDs in active and dormant cells at every moment and calculate the ratios of diffusion constants between active and dormant cells D/D_0 as the averaged MSD ratios over time. The experimental particle radius is converted to a dimensionless number using $a_0 = 10$ nm.

To compare with experiments, we simulate several different volume fractions since the actual volume fraction of bacterial cytoplasm is unknown. Intriguingly, the simulated $D/D_0 - 1$ with $\gamma = 3$ nicely matches the experimental data [Fig. 4(a)], and we will explain the physical mechanism of $\gamma = 3$ later. We find that the simulated diffusion enhancements $D/D_0 - 1$ are insensitive to the volume fraction, although the diffusion constants D and D_0 by themselves change significantly with the volume fraction [Figs. 2(a) and 2(b)]. To confirm the robustness of our results, we also simulate a narrower distribution of particle radii that is more Gaussian-like. The agreement between simulations and experiments is equally valid (Fig. S4). Our results are also independent of the length unit as we choose a different length unit and obtain the same results (Fig. S5). Using the alternative definition of diffusion constants does not affect our conclusions (Fig. S6).

We note that for a dilute active system with $\gamma = 3$, the absolute diffusion constant is a nonmonotonic function of particle size ($D_{\text{dilute}} = 1/\tilde{a} + \tilde{A}\tilde{a}$). Nevertheless, we find that the absolute diffusion constant continuously decreases with particle size in systems with large volume fractions (Fig. S7), consistent with the experimental observations [32].

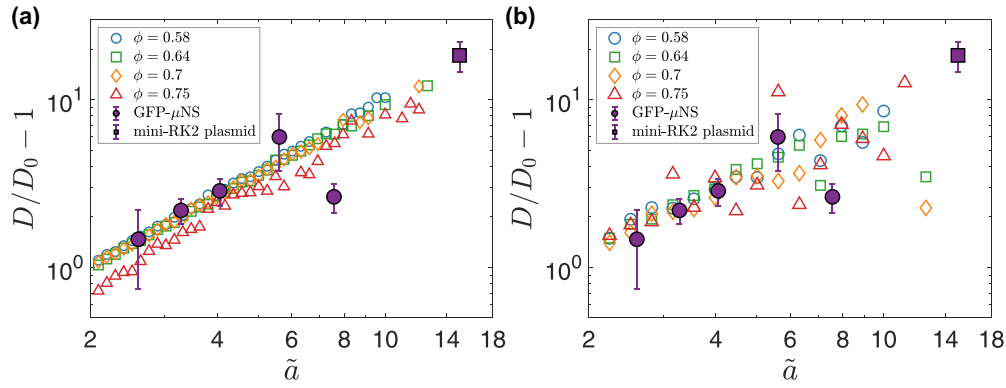


FIG. 4. Comparison between simulations and experiments. (a) The relative enhancements of diffusion constants ($D/D_0 - 1$) from the experimental data match the simulation results of the white-noise active force model. Here, $\gamma = 3$, $\tilde{A} = 0.42$. (b) The same analysis as (a) but for simulations of the self-propelled model with the longer $\Delta\tilde{t}$. Here, $\tilde{F} = 1.38$. The results are binned over particles with a bin interval of 0.02 in (a) and of 0.05 in (b) in the \log_{10} scale. In both panels, $N = 4000$.

We also calculate the radius of gyration, the root-mean-square distance from the center of the trajectory, for both passive and active systems [Fig. S8(a)]. The radii of gyration from simulations decrease linearly with the particle radius in both passive and active systems. The ratio between the passive and active systems also has a linear relationship with the particle radius [Fig. S8(b)]. These results agree with experiments [16], further supporting the validity of our simulations.

In Ref. [16], the authors observed much stronger glasslike properties in dormant cells than in living cells. We find similar hallmarks of a glass transition in our simulations, including dynamic heterogeneity and non-Gaussian displacements [33–35]. The MSDs of particles with similar radii in the same passive system vary over two orders of magnitude [Fig. 5(a)], showing significant dynamic heterogeneity. Meanwhile, this dynamic heterogeneity is much weaker in the corresponding active system. Furthermore, the displacement distributions have a non-Gaussian tail in the passive systems while the deviation from Gaussian distribution is much less significant in the

active systems (Fig. S9). Indeed, the non-Gaussian degree of displacement distributions for large particles is much weaker in the active system than in the passive system [Fig. 5(b)]. Our results show that activity fluidizes the glassy polydisperse system, in agreement with the experimental observations [16]. We find that a higher volume fraction is needed to observe the hallmarks of a glass transition in polydisperse systems (Fig. S10) than in monodisperse systems (Fig. S11), consistent with observations that polydispersity can smear out a glass transition [36].

Mechanism of the cubic scaling $\gamma = 3$. In the following, we explain the cubic scaling of the white-noise active force with the particle radius. We consider a self-propelled model in which an active force with a constant magnitude is exerted on each particle [37–40]. The orientation of this active force is random due to the rotational diffusion of the particle. The equation of motion for the i th active particle becomes

$$\eta_i \frac{dr_{i,\alpha}}{dt} = -\frac{\partial U}{\partial r_{i,\alpha}} + \xi_{i,\alpha} + F n_{i,\alpha}, \quad (6)$$

where F is the magnitude of the active force and $n_{i,\alpha}$ is the orientation vector of the active force in the direction α . The orientation vector \mathbf{n}_i obeys $d\mathbf{n}_i/dt = \mathbf{T}_i \times \mathbf{n}_i$, where \mathbf{T}_i is the thermal random torque. Its autocorrelation function satisfies the FD theorem, $\langle T_{i,\alpha}(t), T_{j,\beta}(t') \rangle = 2D_{R,i} \delta_{ij} \delta_{\alpha\beta} \delta(t - t')$. Here, $D_{R,i} = k_B T / 8\pi \nu a_i^3$ is the rotational diffusion constant for a spherical particle with radius a_i .

At long times, the additional diffusion constant due to activity $D_{\text{active}} = (F/6\pi \nu a)^2 \times (1/2D_R)/3$, where $F/6\pi \nu a$ is the speed of the active particle and $1/2D_R$ is the time for the active force to change its orientation in three-dimensional space. Therefore, the diffusion enhancement of an active particle relative to a passive particle in the dilute limit becomes

$$\frac{D_{\text{dilute}}}{D_{0,\text{dilute}}} = 1 + \frac{2\tilde{F}^2}{9} \tilde{a}^2. \quad (7)$$

Here, \tilde{F} is the dimensionless active force with unit $k_B T/a_0$. Comparing Eqs. (5) and (7), we find that the two models are equivalent in terms of diffusion enhancement when $\gamma = 3$.

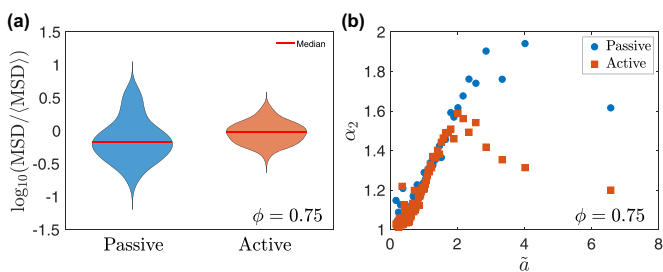


FIG. 5. Activity fluidizes the glassy polydisperse system under a high volume fraction. (a) Violin plot of MSDs of particles whose $\tilde{a} \approx 4$ for passive and active systems under $\phi = 0.75$. The MSDs within a dimensionless time of 1000 are shown in the log scale and normalized by the average value. (b) The non-Gaussian parameter α_2 of the displacement distribution as a function of the particle radius for passive and active systems under $\phi = 0.75$. $\alpha_2 = \langle \Delta \tilde{\mathbf{r}}(\Delta \tilde{t})^4 \rangle / [3 \langle \Delta \tilde{\mathbf{r}}(\Delta \tilde{t})^2 \rangle^2]$ and it equals 1 if the displacements obey the Gaussian distribution. The results are averaged with 50 particles in each bin. The maximum α_2 is shown from $\Delta \tilde{t} = 50$ to 2500. For the active systems, $\tilde{A} = 0.42$ and $\gamma = 3$. In both panels, $N = 4000$.

This conclusion applies to the dilute limit, and we hypothesize that the equivalence of the two models is still valid under high-volume fractions.

To test our hypothesis, we simulate the self-propelled model with \bar{F} satisfying $\bar{A} = 2\bar{F}^2/9$ so that the two models lead to the same diffusion enhancement in the dilute limit. The agreement between simulations and experimental data also holds for the self-propelled model [Fig. 4(b)]. We use the longer $\Delta\tilde{t}$ and confirm that the $\Delta\tilde{t}$ calculated in this way is longer than the rotational relaxation time. We find that the magnitude of the active force $F = 0.57$ pN in the physical unit, consistent with typical force magnitudes in the cytoplasm [28]. We remark that the constant magnitude of the active force is crucial to obtain the correct scaling of diffusion enhancement. In an alternative model with a constant active speed, $D_{\text{dilute}}/D_{0,\text{dilute}} - 1 \sim \bar{a}^4$, inconsistent with experiments. In a more biologically plausible scenario, the magnitude of the active force can be random among different particles [41]. Therefore, we also simulate a modified model in which the active force obeys a size-independent normal distribution and obtain similar results (Fig. S12), further strengthening our proposed mechanism.

Discussion. In this Letter, we introduce a white-noise active force to a highly polydisperse system to mimic bacterial cytoplasm. While prior works have investigated the effect of activities on particle mobility [42–44], our work simultaneously incorporates crowding by different particle sizes and active forces. Due to its out-of-equilibrium nature, the FD theorem does not constrain the active random force. Surprisingly, a white-noise active force reproduces the experimentally measured ratios of diffusion constants between living and dormant bacteria with its autocorrelation function proportional to the cube of the particle radius. We note that an active random force generally generates an additional friction coefficient that is inversely proportional to an active temperature [27,45–47]. We show that the additional friction coefficient does not affect our conclusions because the active temperature is typically

much higher than the thermal temperature (see Supplemental Material [31]).

We further demonstrate that the white-noise active force model with $\gamma = 3$ is equivalent to the self-propelled model with a constant-magnitude active force regarding the diffusion enhancement. Our results suggest an emergent simplicity when many active processes are averaged simultaneously. Importantly, we identify the magnitude of the active force, $F = 0.57$ pN. While the origin of this active force is still unclear [16], we hypothesize that it may come from the collision of small molecules with proteins, e.g., amino acids and ions, which are out of equilibrium [45]. We note that the active force can be estimated as the thermal energy divided by typical protein sizes, $F = k_B T/a \approx 0.4$ pN, where a is the typical size of proteins around 10 nm. The active force applied to proteins is just enough to overcome thermal fluctuation. This particular magnitude of active force allows proteins to move or change their configurations according to some specific intracellular signaling. On the other hand, it lets proteins quickly change their dynamics when the signaling changes. Therefore, the magnitude of the active force around the pN range may be evolutionarily selected.

We note that the time-averaged MSDs of particles of the same size differ among independent simulations. Nevertheless, the MSD averaged over the time-averaged MSDs of independent simulations are close to the ensemble-averaged MSD (Fig. S13), suggesting a weak nonergodicity effect, presumably because polydispersity smears out the glass transition (Fig. S11). Finally, we remark that while a hydrodynamic interaction has been shown to reduce the diffusion coefficient, its effect may be negligible for particles with a radius above 25 nm that we use to compare with experimental data [22].

Acknowledgments. We thank Yiyang Ye, Hua Tong, Sheng Mao, and Ming Han for helpful discussions related to this work. The research was funded by National Key R&D Program of China (2021YFF1200500) and supported by grants from Peking-Tsinghua Center for Life Sciences.

-
- [1] P. H. von Hippel and O. G. Berg, Facilitated target location in biological systems, *J. Biol. Chem.* **264**, 675 (1989).
- [2] M. B. Elowitz, M. G. Surette, P.-E. Wolf, J. B. Stock, and S. Leibler, Protein mobility in the cytoplasm of *Escherichia coli*, *J. Bacteriol.* **181**, 197 (1999).
- [3] A. Chari and U. Fischer, Cellular strategies for the assembly of molecular machines, *Trends Biochem. Sci.* **35**, 676 (2010).
- [4] J. T. Mika and B. Poolman, Macromolecule diffusion and confinement in prokaryotic cells, *Curr. Opin. Biotechnol.* **22**, 117 (2011).
- [5] S. Cayley, Jr., B. A. Lewis, H. J. Guttman, and M. T. Record, Jr., Characterization of the cytoplasm of *Escherichia coli* K-12 as a function of external osmolarity: Implications for protein-DNA interactions *in vivo*, *J. Mol. Biol.* **222**, 281 (1991).
- [6] S. B. Zimmerman and S. O. Trach, Estimation of macromolecule concentrations and excluded volume effects for the cytoplasm of *Escherichia coli*, *J. Mol. Biol.* **222**, 599 (1991).
- [7] R. Swaminathan, C. P. Hoang, and A. Verkman, Photobleaching recovery and anisotropy decay of green fluorescent protein GFP-S65T in solution and cells: Cytoplasmic viscosity probed by green fluorescent protein translational and rotational diffusion, *Biophys. J.* **72**, 1900 (1997).
- [8] R. J. Ellis, Macromolecular crowding: obvious but underappreciated, *Trends Biochem. Sci.* **26**, 597 (2001).
- [9] R. Milo and R. Phillips, *Cell Biology by the Numbers* (Garland Science, New York, 2015).
- [10] J. A. Dix and A. Verkman, Crowding effects on diffusion in solutions and cells, *Annu. Rev. Biophys.* **37**, 247 (2008).
- [11] H.-X. Zhou, G. Rivas, and A. P. Minton, Macromolecular crowding and confinement: Biochemical, biophysical, and potential physiological consequences, *Annu. Rev. Biophys.* **37**, 375 (2008).
- [12] I. Golding and E. C. Cox, Physical Nature of Bacterial Cytoplasm, *Phys. Rev. Lett.* **96**, 098102 (2006).
- [13] A. Nenninger, G. Mastroianni, and C. W. Mullineaux, Size dependence of protein diffusion in the cytoplasm of *Escherichia coli*, *J. Bacteriol.* **192**, 4535 (2010).
- [14] K. A. Dill, K. Ghosh, and J. D. Schmit, Physical limits of cells and proteomes, *Proc. Natl. Acad. Sci. USA* **108**, 17876 (2011).

- [15] S. C. Weber, A. J. Spakowitz, and J. A. Theriot, Nonthermal ATP-dependent fluctuations contribute to the *in vivo* motion of chromosomal loci, *Proc. Natl. Acad. Sci. USA* **109**, 7338 (2012).
- [16] B. Parry, I. Surovtsev, M. Cabeen, C. O'Hern, E. Dufresne, and C. Jacobs-Wagner, The bacterial cytoplasm has glass-like properties and is fluidized by metabolic activity, *Cell* **156**, 183 (2014).
- [17] M. Guo, A. Ehrlicher, M. Jensen, M. Renz, J. Moore, R. Goldman, J. Lippincott-Schwartz, F. Mackintosh, and D. Weitz, Probing the stochastic, motor-driven properties of the cytoplasm using force spectrum microscopy, *Cell* **158**, 822 (2014).
- [18] M. C. Munder, D. Midtvedt, T. Franzmann, E. Nuske, O. Otto, M. Herbig, E. Ulbricht, P. Müller, A. Taubenberger, S. Maharana *et al.*, A pH-driven transition of the cytoplasm from a fluid-to a solid-like state promotes entry into dormancy, *eLife* **5**, e09347 (2016).
- [19] R. P. Joyner, J. H. Tang, J. Helenius, E. Dultz, C. Brune, L. J. Holt, S. Huet, D. J. Müller, and K. Weis, A glucose-starvation response regulates the diffusion of macromolecules, *eLife* **5**, e09376 (2016).
- [20] N. Chebotareva, B. Kurganov, and N. Livanova, Biochemical effects of molecular crowding, *Biochemistry (Moscow)* **69**, 1239 (2004).
- [21] D. J. Bicout and M. J. Field, Stochastic dynamics simulations of macromolecular diffusion in a model of the cytoplasm of *Escherichia coli*, *J. Phys. Chem.* **100**, 2489 (1996).
- [22] T. Ando and J. Skolnick, Crowding and hydrodynamic interactions likely dominate *in vivo* macromolecular motion, *Proc. Natl. Acad. Sci. USA* **107**, 18457 (2010).
- [23] S. R. McGuffee and A. H. Elcock, Diffusion, crowding & protein stability in a dynamic molecular model of the bacterial cytoplasm, *PLoS Comput. Biol.* **6**, e1000694 (2010).
- [24] C. Wilhelm, Out-of-Equilibrium Microrheology inside Living Cells, *Phys. Rev. Lett.* **101**, 028101 (2008).
- [25] F. S. Gnesotto, F. Mura, J. Gladrow, and C. P. Broedersz, Broken detailed balance and non-equilibrium dynamics in living systems: a review, *Rep. Prog. Phys.* **81**, 066601 (2018).
- [26] A. P. Solon, J. Stenhammar, R. Wittkowski, M. Kardar, Y. Kafri, M. E. Cates, and J. Tailleur, Pressure and Phase Equilibria in Interacting Active Brownian Spheres, *Phys. Rev. Lett.* **114**, 198301 (2015).
- [27] A. P. Solon, Y. Fily, A. Baskaran, M. E. Cates, Y. Kafri, M. Kardar, and J. Tailleur, Pressure is not a state function for generic active fluids, *Nat. Phys.* **11**, 673 (2015).
- [28] P. Roca-Cusachs, V. Conte, and X. Trepats, Quantifying forces in cell biology, *Nat. Cell Biol.* **19**, 742 (2017).
- [29] M. Doi, *Soft Matter Physics* (Oxford University Press, Oxford, UK, 2013).
- [30] G. L. Hunter and E. R. Weeks, The physics of the colloidal glass transition, *Rep. Prog. Phys.* **75**, 066501 (2012).
- [31] See Supplemental Material at <http://link.aps.org/supplemental/10.1103/PhysRevResearch.5.L032018> for additional discussions and figures.
- [32] M. Kumar, M. S. Mommer, and V. Sourjik, Mobility of cytoplasmic, membrane, and dna-binding proteins in *Escherichia coli*, *Biophys. J.* **98**, 552 (2010).
- [33] A. H. Marcus, J. Schofield, and S. A. Rice, Experimental observations of non-Gaussian behavior and stringlike cooperative dynamics in concentrated quasi-two-dimensional colloidal liquids, *Phys. Rev. E* **60**, 5725 (1999).
- [34] E. R. Weeks, J. C. Crocker, A. C. Levitt, A. Schofield, and D. A. Weitz, Three-dimensional direct imaging of structural relaxation near the colloidal glass transition, *Science* **287**, 627 (2000).
- [35] W. K. Kegel and A. van Blaaderen, Direct observation of dynamical heterogeneities in colloidal hard-sphere suspensions, *Science* **287**, 290 (2000).
- [36] E. Zaccarelli, S. M. Liddle, and W. C. Poon, On polydispersity and the hard sphere glass transition, *Soft Matter* **11**, 324 (2015).
- [37] J. R. Howse, R. A. L. Jones, A. J. Ryan, T. Gough, R. Vafabakhsh, and R. Golestanian, Self-Motile Colloidal Particles: From Directed Propulsion to Random Walk, *Phys. Rev. Lett.* **99**, 048102 (2007).
- [38] Y. Fily and M. C. Marchetti, Athermal Phase Separation of Self-Propelled Particles with No Alignment, *Phys. Rev. Lett.* **108**, 235702 (2012).
- [39] J. Bialké, T. Speck, and H. Löwen, Crystallization in a Dense Suspension of Self-Propelled Particles, *Phys. Rev. Lett.* **108**, 168301 (2012).
- [40] G. S. Redner, M. F. Hagan, and A. Baskaran, Structure and Dynamics of a Phase-Separating Active Colloidal Fluid, *Phys. Rev. Lett.* **110**, 055701 (2013).
- [41] M. Xu, J. L. Ross, L. Valdez, and A. Sen, Direct Single Molecule Imaging of Enhanced Enzyme Diffusion, *Phys. Rev. Lett.* **123**, 128101 (2019).
- [42] R. Mandal, P. J. Bhuyan, M. Rao, and C. Dasgupta, Active fluidization in dense glassy systems, *Soft Matter* **12**, 6268 (2016).
- [43] C. Yuan, A. Chen, B. Zhang, and N. Zhao, Activity-crowding coupling effect on the diffusion dynamics of a self-propelled particle in polymer solutions, *Phys. Chem. Chem. Phys.* **21**, 24112 (2019).
- [44] L. Abbaspour and S. Klumpp, Enhanced diffusion of a tracer particle in a lattice model of a crowded active system, *Phys. Rev. E* **103**, 052601 (2021).
- [45] A. Solon and J. M. Horowitz, On the Einstein relation between mobility and diffusion coefficient in an active bath, *J. Phys. A: Math. Theor.* **55**, 184002 (2022).
- [46] A. Shakerpoor, E. Flenner, and G. Szamel, The Einstein effective temperature can predict the tagged active particle density, *J. Chem. Phys.* **154**, 184901 (2021).
- [47] O. Granek, Y. Kafri, and J. Tailleur, Anomalous Transport of Tracers in Active Baths, *Phys. Rev. Lett.* **129**, 038001 (2022).